Optimal State Estimation for Systems Driven by Jump–Diffusion Process With Application to Road Anomaly Detection

Zhaojian Li, *Member, IEEE*, Ilya V. Kolmanovsky, *Fellow, IEEE*, Uroš V. Kalabić, *Member, IEEE*, Ella M. Atkins, *Senior Member, IEEE*, Jianbo Lu, *Senior Member, IEEE*, and Dimitar P. Filev, *Fellow, IEEE*

***Abstract*— Jump–diffusion processes (JDPs) involve a combination of jumps (Poisson process) and diffusions (Wiener process). JDPs can be used to model large classes of disturbances in engineering applications, such as road disturbances to a car, wind disturbances to an airplane, and system parameter perturbations. This paper develops a road anomaly detector by exploiting an optimal state estimator for systems driven by JDP in combination with the multi-input observer. State estimation with the JDP-based estimator is shown to have better performance than a Kalman filter when jumps, such as potholes and bumps, are present. The road anomaly detector is implemented in an experimental test vehicle and its experimental validation results are reported.**

***Index Terms*— Jump–diffusion process (JDP), road anomaly detection, state estimation.**

I. Introduction

THE DIFFUSION (or Wiener) processes have traditionally been used to model stochastic disturbances in control systems. However, rare but pronounced events (such as a car hitting a pothole or an aircraft encountering a wind gust) may be better modeled with jump (or Poisson) processes. Jump–diffusion processes (JDPs), involving both jumps and diffusions, can thus be used to model many engineering disturbances.

Jump–diffusion models have primarily been used in the past to represent asset pricing in finance [1]–[4]. In this paper, we consider the problem of designing a state estimator for systems driven by jump–diffusion disturbances and we develop a road anomaly detector by exploiting the JDP-based state estimator in combination with the multi-input observer.

Road anomaly information can be used to warn drivers, notify road maintenance crews, and enhance vehicle suspension control [5]. Road anomaly detection has attracted great attention in the past decade. In [6], a pothole detector is developed using three external accelerometers with machine learning techniques. In [7], a pothole-detection algorithm is proposed by developing and exploiting a multiphase dynamic model. High-bandwidth sensors are required in [7] for successful identification. Recently, Jaguar and Land Rover have launched a "Pothole Alert" project with the goal of detecting potholes with onboard vehicle sensors [8].

In this paper, we develop a novel framework to detect and classify road anomalies with commonly available vehicle sensors. A front half-car dynamic model is developed to characterize vehicle-road interaction. In this model, the roadway velocity disturbances at the two wheels are treated as inputs and a multi-input observer developed in [9] is used to estimate the inputs. The input observer implementation requires the estimates of system states, and the JDP-based estimator is exploited to estimate these states. We demonstrate that the JDP-based estimator outperforms a Kalman filter when jumps, such as potholes and bumps, are present. A road anomaly detection algorithm is further developed and implemented in a Lincoln MKS test vehicle. Performance evaluation results are reported.

The contributions of this paper include the following. First, the JDP-based disturbance modeling is for the first time exploited in a comprehensive way in the context of engineering application. Previously, JDP models were mainly used for price modeling in finance. Second, an optimal state estimator is developed for linear systems with JDP disturbances. Third, a road anomaly detector is developed by exploiting the JDP-based state estimator. This road anomaly detector is implemented in an experimental vehicle in real time, and promising experimental results are reported. Compared with the conference paper [10], in this paper, we present more comprehensive results on the JDP estimator properties with complete proofs. In particular, we extend the treatment to the vector disturbance case.

Manuscript received July 10, 2016; accepted October 16, 2016. Manuscript received in final form October 16, 2016. This work was supported by Ford Motor Company-The University of Michigan Alliance. Recommended by Associate Editor M. Tanelli.

Z. Li, I. V. Kolmanovsky, and E. M. Atkins are with the Department of Aerospace Engineering, University of Michigan, Ann Arbor, MI 48105 USA (e-mail: zhaojli@umich.edu; ilya@umich.edu; ematkins@umich.edu).

U. V. Kalabić was with the Department of Aerospace Engineering, University of Michigan, Ann Arbor, MI 48105 USA. He is now with Mitsubishi Electric Research Laboratories, Cambridge, MA 02139 USA (e-mail: kalabic@umich.edu).

J. Lu and D. P. Filev are with Research and Advanced Engineering, Ford Motor Company, Dearborn, MI 48121 USA (e-mail: jlu10@ford.com; dfilev@ford.com).

Color versions of one or more of the figures in this paper are available online at http://ieeexplore.ieee.org.

Digital Object Identifier 10.1109/TCST.2016.2620062

This paper is organized as follows. Section II reviews the background results about systems driven by JDP. Section III presents the detailed system design of the anomaly detection algorithm from perspectives of dynamic modeling, input observer, JDP-based state estimation, and detection logics. Experimental results are reported in Section IV. Finally, concluding remarks are made in Section V.

II. Systems Driven by Jump–Diffusion Processes

The JDP is a combination of a jump process and a diffusion process. The jump portion, $\eta(t)$, of a JDP is modeled by a Poisson process, which implies that the number of jumps in a time interval of length Δt, $N(\Delta t)$, is distributed as

$$\text{Prob}\big(N(\Delta t) = k\big) = e^{-\lambda \Delta t}\frac{(\lambda \Delta t)^k}{k!} \tag{1}$$

where λ is a rate parameter. During a small time interval of length Δt, the probability that $\eta(t)$ may jump upward is approximately equal to $\lambda \Delta t$; with the probability approximately equal to $1 - \lambda \Delta t$, $\eta(t)$ retains a constant value. The probability of encountering more than one jump during a small time interval Δt is $o(\Delta t)$, and the numbers of jumps in any two disjoint time intervals are independent [11]. It can be shown that the expected time between two consecutive jumps is equal to $1/\lambda$. The jump *size* of $\eta(t)$ can also be a random variable; such a Poisson process is often referred to as a *compound Poisson process*.

A scalar JDP has the form, $\eta + \sigma_\zeta \cdot \zeta$, $\sigma_\zeta > 0$, where η is a Poisson process and ζ is a standard Wiener process. Since both Wiener process and Poisson process are Markov processes, the JDP is also a Markov process [12], [13]. A sample trajectory of a system, $\dot{x}(t) = a(x(t)) + b(x(t)) \cdot w(t)$, with $w = \dot{\eta} + \sigma_\zeta \cdot \dot{\zeta}$, can be approximated using discrete time updates as

$$\Delta x(t) = a(x(t)) \cdot \Delta t + b(x(t)) \cdot \Delta w(t)$$
$$\Delta w(t) = \begin{cases} \Delta \eta^k + \sqrt{\Delta t} \cdot \mathcal{N}(0,1) \cdot \sigma_\zeta, & \text{if } t = \tau_k \\ \sqrt{\Delta t} \cdot \mathcal{N}(0,1) \cdot \sigma_\zeta, & \text{if } t \neq \tau_k \end{cases}$$

where Δt is the time increment, $\Delta x(t)$ is the state increment, and $\mathcal{N}(0,1)$ denotes a random number generated from a normal distribution with zero mean and unit variance. $\Delta \eta^k$ is the random size of the kth jump occurring at a random time instant τ_k. Using standard notations in the stochastic control literature, the above system is written as

$$dx = a(x(t))dt + b(x(t)) \cdot (d\eta + \sigma_\zeta d\zeta).$$

Consider now a stochastic system in the following form:

$$dx(t) = [A(t)x(t) + f(t)]dt + D(t,x)d\zeta + G(t,x)d\eta \tag{2}$$

where A, D, and G are known (matrix) functions of appropriate dimensions, f is a known function, ζ is a standard vector Wiener process, and η is a vector jump process, i.e., each component is a scalar jump process. We assume that each component of the vector η has the same rate parameter. The processes η and ζ are assumed to be independent of each other. The infinitesimal generator of a given sufficiently smooth function $V(t,x)$, denoted by $LV(t,x)$, can be shown to have the following form [14]:

$$\begin{aligned} LV(t,x) = {} & \frac{\partial V}{\partial t} + [A(t)x(t) + f(t)]^T V_x'(t,x) \\ & + \frac{1}{2}\text{trace}(D(t,x)^T V_{xx}'' D(t,x)) \\ & + \int_{\mathbb{R}^m} [V(t, x + G(t,x)s) - V(t,x)]\lambda \phi(s) ds \end{aligned} \tag{3}$$

where m is the dimension of η, V_x' and V_{xx}'' denote the first and second partial derivatives of V with respect to x, λ is the rate parameter of the jumps, and $\phi(s)$ is the joint jump size probability density function, assuming hereafter that the jump size is a continuous random vector.

Under appropriate assumptions [14], [15], Dynkin's formula applies and

$$E[V(t,x(t))] - E[V(0,x(0))] = E\int_0^t [LV(\tau, x(\tau))]d\tau \tag{4}$$

where E denotes the expectation.

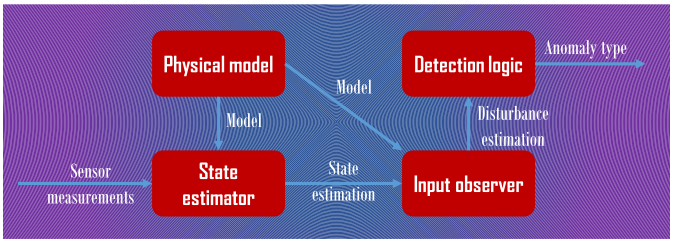

Fig. 1. Schematic system flowchart for pothole-detection design.

III. Road Anomaly Detection and Classification

In this paper, we develop a model-based road anomaly detection algorithm that not only detects road anomalies but also labels the anomaly types, such as potholes, speed bumps, and road joints.

When vehicles travel on roads, they are perturbed by road disturbances. In suspension control applications, roadway vertical velocity disturbances are typically modeled as inputs to the suspension system [5], [16], [17]. Note that road anomalies (e.g., potholes and speed bumps) correspond to large disturbance jumps. Therefore, if we can estimate these road disturbances, road anomalies can then be detected by identifying big jumps.

Consider the overall vehicle as a system, then the road disturbances at the four wheels can be treated as inputs to the system. Hence, input observers can be exploited to estimate the road disturbances. A schematic chart of the system design is shown in Fig. 1.

In this paper, we exploit the input observer from [9] to estimate road inputs. This input observer requires full-state information, and a JDP-based state estimator is developed to estimate system states from sensor measurements. Both the input observer and state estimator are model-based. With the estimated road disturbances from the input observer, detection

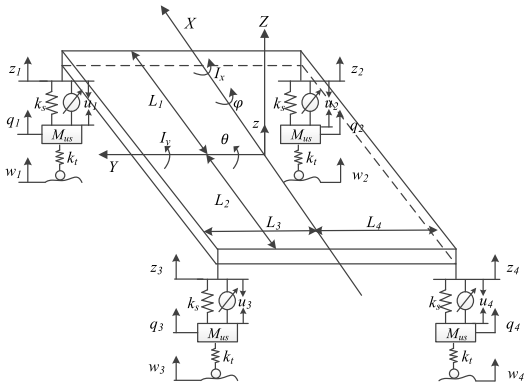

Fig. 2. Seven DoF full-car model schematics.

Fig. 3. Test vehicle and main available sensors.

logics are applied to determine anomaly existence and type. Sections III-A–III-D correspond to each of the blocks in Fig. 1.

A. Dynamic Model

To implement the input observer based on the approach in [9], a dynamic model is required. We initially used the full-car model from Fig. 2. The model has seven degrees of freedom (DoFs) and fourteen states. This comprehensive model can capture the disturbances at all four wheels. However, its use is impeded by the number of available sensors in our test vehicle, a 2012 Lincoln MKS, as shown in Fig. 3. In this vehicle, only four sensor measurements (left front suspension deflection, left rear suspension deflection, vertical acceleration, and roll rate) are available. Using these sensor measurements, our simulation results reveal that some of the full-car model states cannot be accurately estimated.

A reduced front half-car model, shown in Fig. 4, is used as an alternative model for the design of the input observer. The front half car is modeled as a rigid body with mass m_b. I_x represents the moment of inertia about the longitudinal axis. The variables z, z_1, and z_2 represent the vertical displacement of the center of gravity (CG), left body tip, and right body tip, respectively, from equilibrium. The left and right tip-to-CG distances are denoted by L_1 and L_2, respectively. The parameters k_s and c_s represent the spring stiffness and damping coefficient of the suspension system, respectively, and we

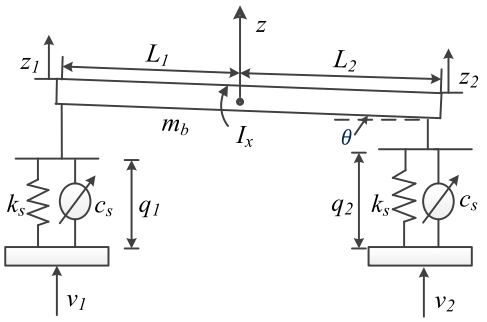

Fig. 4. Two DoF half-car model.

assume that the left and right sides have the same parameters. We denote the roll angle by θ. The variables q_1 and q_2 represent the left and right suspension deflections from equilibrium values, respectively. The signals v_1 and v_2 are the road velocity inputs to the left and right wheels, respectively. Note that since the wheel has high stiffness, to simplify the model, we consider v_1 and v_2 as being directly applied to the left and right suspensions, respectively.

Defining $x_1 = q_1$, $x_2 = q_2$, $x_3 = \dot{z}$, and $x_4 = \dot{\theta}$ as the states, we obtain the following equations of motion:

$$\begin{aligned}
\dot{x}_1 &= x_3 + L_1 x_4 - v_1 \\
\dot{x}_2 &= x_3 - L_2 x_4 - v_2 \\
\frac{1}{2} m_b \dot{x}_3 &= -k_s x_1 - c_s \dot{x}_1 - k_s x_2 - c_s \dot{x}_2 \\
\frac{1}{2} I_x \dot{x}_4 &= -L_1 k_s x_1 - L_1 c_s \dot{x}_1 + L_2 k_s x_2 + L_2 c_s \dot{x}_2.
\end{aligned} \tag{5}$$

The measurement vector y includes front left suspension deflection q_1, vertical acceleration $\ddot{z}$, and roll rate $\dot{\theta}$, that is

$$y = [q_1 \quad \ddot{z} \quad \dot{\theta}]^T. \tag{6}$$

Let $w = [v_1 \quad v_2]^T$ represent the input vector. The equations of motion in (5) can be represented as

$$\begin{aligned}
\dot{x} &= Ax + \Gamma w \\
y &= Cx + Dw + D_2 v
\end{aligned} \tag{7}$$

where v is the measurement noise and A, Γ, C, and D are the constant matrices consistent with (5) and (6).

B. Input Observer

To estimate the road input w in (7), we exploit a multi-input observer using the approach developed in [9]. For the half-car dynamics in (7), the model can be written as

$$\dot{x}(t) = Ax(t) + \Gamma w(t). \tag{8}$$

The input observer has the following form:

$$\begin{aligned}
\dot{\varepsilon}(t) &= -\gamma S \varepsilon(t) + \gamma SAx(t) + (\gamma S)^2 Kx(t) \\
\hat{w}(t) &= -\varepsilon(t) + \gamma SKx(t)
\end{aligned} \tag{9}$$

where ε is the observer state, $\gamma > (1/2)$ is a scalar gain, and $S = (1/2)\mathbf{I}_m + (1/2\gamma)P$, where P is a weighting matrix, m is the number of inputs, and $K = (\Gamma^T \Gamma)^{-1} \Gamma^T$ is the pseudoinverse of Γ. Note that the column rank of Γ

must be equal to m, so that K is well defined. Henceforth, we assume that $P = \mathbf{I}_m$.

In [9], it is shown that, assuming $\|\dot{w}(t)\| \leq b_1$, the estimation error is bounded by

$$\|w(t) - \hat{w}(t)\|_P^2 \leq \|w(0) - \hat{w}(0)\|_P^2 e^{-\gamma t} + \frac{b_1^2}{2\gamma^2}. \quad (10)$$

Note that to implement the input observer in (9), we require full-state information. Since not all the states are measured, a state estimator is needed to estimate x from measurements y in (6). In Section III-C, we exploit the JDP-based state estimator for state estimation. Compared with Kalman filter, the conventional treatment of the road velocity input as Gaussian noise is enhanced with a JDP model that is able to account for rare but pronounced events, such as potholes and bumps.

C. Optimal State Estimation for Systems Driven by Jump–Diffusion Process

In this section, we design an optimal state estimator for the dynamic system (7). A conventional choice of state estimator is the Kalman filter, which assumes that the disturbance w is Gaussian. However, road anomalies, such as potholes and speed bumps, are pronounced events to account for which a more general representation of the disturbance w is desired. In this paper, we model the road disturbance as a JDP. This general representation can model both normal roads and road anomalies, such as potholes and speed bumps.

1) JDP-Based State Estimation: Consider the following stochastic system:

$$dx = Axdt + Budt + \Gamma[d\eta + \sigma_\zeta d\zeta] \quad (11)$$

where x is a vector state, u is a known input, and η is a vector jump process with each component having the same rate parameter λ. The joint probability density function of the jump sizes of η is denoted by $\phi(\cdot)$. In 11, ζ is a standard vector Wiener process, and $\sigma_\zeta \sigma_\zeta^T$ is a positive-definite matrix. We let μ_η and Σ_η denote, respectively, the jump size mean and covariance. The jump sizes are assumed to be independent and identically distributed. System (11) can also be written conventionally as

$$\dot{x} = Ax + Bu + \Gamma w \quad (12)$$

with $w = \dot{\eta} + \sigma_\zeta \dot{\zeta}$. The objective is to estimate states of system (11) from output measurements satisfying

$$y = Cx + Dw + D_2 \nu \quad (13)$$

where $\nu = \sigma_\xi \dot{\xi}$, ξ is a standard vector Wiener process representing the sensor noise, and the matrix $\sigma_\xi \sigma_\xi^T$ is positive-definite. The processes η, ζ, and ξ are assumed to be independent. Note that (12) and (13) are a more general form of (7) with $u \neq 0$.

The state estimator for system (12) based on the output measurement (13) is assumed to be of the form

$$\begin{aligned}\dot{\hat{x}} &= A\hat{x} + Bu + F(\hat{y} - y) + (\Gamma + FD)\lambda\mu_\eta \\ &= A\hat{x} + Bu + F(C\hat{x} - Cx - Dw - D_2\nu) \\ &\quad + (\Gamma + FD)\lambda\mu_\eta \end{aligned} \quad (14)$$

where F is the estimator gain to be determined. Let $e = x - \hat{x}$ denote the estimation error. Then

$$\dot{e} = (A + FC)e + (\Gamma + FD)w + FD_2\nu - (\Gamma + FD)\lambda\mu_\eta. \quad (15)$$

Defining $\bar{D} = [FD_2\sigma_\xi \quad (\Gamma + FD)\sigma_\zeta]$, we have

$$\begin{aligned} de = &[(A + FC)e - (\Gamma + FD)\lambda\mu_\eta]dt \\ &+ \bar{D}\begin{bmatrix} d\xi \\ d\zeta \end{bmatrix} + (\Gamma + FD)d\eta. \end{aligned} \quad (16)$$

Let $z = Se$ be a weighted estimation error we want to keep small. We select F to minimize

$$J = \lim_{t\to\infty} \frac{1}{t} E \int_0^t z^T(\tau) z(\tau) d\tau. \quad (17)$$

The optimal gain F that minimizes (17) is given in Theorem 1.

Theorem 1: Suppose the pair (A, C) is detectable, the pair (A, Γ) is stabilizable, $D_2 D_2^T > 0$ and $S^T S > 0$. Then, the optimal gain F that minimizes (17) in the open set of all gains F for which $(A+FC)$ is asymptotically stable (Hurwitz), is given by

$$F = -\Gamma\bar{\Sigma}D^T V_2^{-1} - QC^T V_2^{-1} \quad (18)$$

and Q is the unique positive semidefinite solution to

$$\begin{aligned}(A - \Gamma\bar{\Sigma}D^T V_2^{-1}C)Q + Q\big(A - \Gamma\bar{\Sigma}D^T V_2^{-1}C\big)^T \\ + V_1 - QC^T V_2^{-1} CQ = 0 \end{aligned} \quad (19)$$

where $V_1 = \Gamma\bar{\Sigma}\Gamma^T - \Gamma\bar{\Sigma}D^T V_2^{-1} D\bar{\Sigma}\Gamma^T$, $V_2 = D_2\sigma_\xi\sigma_\xi^T D_2^T + D\bar{\Sigma}D^T$, and $\bar{\Sigma} = \sigma_\zeta\sigma_\zeta^T + \lambda\mu_\eta\mu_\eta^T + \lambda\Sigma_\eta$, where Σ_η is the covariance of η.

Proof: Since (A, C) is detectable, there exists F, such that $A + FC$ is asymptotically stable. Assuming that $\bar{A} = A + FC$ is asymptotically stable, and given that $S^T S > 0$, we can find $M > 0$ such that

$$M\bar{A} + \bar{A}^T M = -S^T S. \quad (20)$$

Let $V = (1/2)e^T Me$. From (3)

$$\begin{aligned} LV &= [\bar{A}e - (\Gamma + FD)\lambda\mu_\eta]^T Me + \frac{1}{2}\text{trace}(\bar{D}^T M\bar{D}) \\ &\quad + \int_{\mathbb{R}^m} \left[\frac{1}{2}s^T(\Gamma + FD)^T M(\Gamma + FD)s \right. \\ &\qquad \left. + e^T M(\Gamma + FD)s\right]\lambda\phi(s)ds \\ &= \frac{1}{2}e^T(\bar{A}^T M + M\bar{A})e + \frac{1}{2}\text{trace}(\bar{D}^T M\bar{D}) \\ &\quad + \frac{1}{2}\lambda\cdot\text{trace}[(\Gamma + FD)^T M(\Gamma + FD)\Sigma_\eta] \\ &\quad + \frac{1}{2}\lambda\cdot\mu_\eta^T(\Gamma + FD)^T M(\Gamma + FD)\mu_\eta \\ &= -\frac{1}{2}e^T S^T Se + \frac{1}{2}\text{trace}(\bar{D}^T M\bar{D}) \\ &\quad + \frac{1}{2}\tilde{D}^T M\tilde{D} + \frac{1}{2}\text{trace}[\hat{D}^T M\hat{D}] \end{aligned} \quad (21)$$

where $\tilde{D} = \sqrt{\lambda}(\Gamma + FD)\mu_\eta$ and $\hat{D} = \sqrt{\lambda}(\Gamma + FD)N$ with $NN^T = \Sigma_\eta$ being a lower triangular matrix from Cholesky decomposition.

This expression, along with $S^T S > 0$ and $M > 0$, implies that $E[V(t)]$ is bounded. Then, using Dynkin's formula

$$\begin{aligned}\frac{1}{t}E[V(t)] - \frac{1}{t}E[V(0)] \\ = -\frac{1}{2}\frac{1}{t}E\int_0^t z^T(\tau)z(\tau)d\tau + \frac{1}{2}\tilde{D}^T M\tilde{D} \\ + \frac{1}{2}\text{trace}(\bar{D}^T M\bar{D}) + \frac{1}{2}\text{trace}(\hat{D}^T M\hat{D}). \end{aligned} \quad (22)$$

Consequently

$$\begin{aligned}\lim_{t\to\infty}\frac{1}{t}E\int_0^t z^T(\tau)z(\tau)d\tau \\ = \tilde{D}^T M\tilde{D} + \text{trace}(\bar{D}^T M\bar{D}) + \text{trace}(\hat{D}^T M\hat{D}). \end{aligned} \quad (23)$$

Next, apply the method of indeterminate Lagrangian multipliers. There exist $\lambda_0 \in \{0, 1\}$ and a matrix Q, $(\lambda_0, Q) \neq 0$ which together with the optimal values of F and M, yield the first-order optimality conditions for function J from (17)

$$\begin{aligned} J &= \lambda_0[\text{trace}(\bar{D}\bar{D}^T M) + \text{trace}(\tilde{D}\tilde{D}^T M) \\ &\quad + \text{trace}(\hat{D}\hat{D}^T M)] + \text{trace}\big[(M\bar{A} + \bar{A}^T M + S^T S)Q\big] \\ &= \text{trace}\big[\big(FD_2\sigma_\xi\sigma_\xi^T D_2^T F^T + (\Gamma+FD)\sigma_\zeta\sigma_\zeta^T(\Gamma+FD)^T\big)M\big] \\ &\quad + \text{trace}\big[\lambda\cdot(\Gamma+FD)\mu_\eta\mu_\eta^T(\Gamma+FD)^T M\big] \\ &\quad + \text{trace}\big[\lambda\cdot(\Gamma+FD)\Sigma_\eta^T(\Gamma+FD)^T M\big] \\ &\quad + \text{trace}[(M\bar{A} + \bar{A}^T M + S^T S)Q] \\ &= \text{trace}\big(FD_2\sigma_\xi\sigma_\xi^T D_2^T F^T M\big) \\ &\quad + \text{trace}[(\Gamma+FD)\bar{\Sigma}(\Gamma+FD)^T M] \\ &\quad + \text{trace}[(M\bar{A} + \bar{A}^T M + S^T S)Q] \end{aligned} \quad (24)$$

where $\bar{\Sigma} = \sigma_\zeta\sigma_\zeta^T + \lambda\mu_\eta\mu_\eta^T + \lambda\Sigma_\eta$. Therefore

$$\begin{aligned}\frac{\partial J}{\partial F} &= 2MFD_2\sigma_\xi\sigma_\xi^T D_2^T + 2M\Gamma\bar{\Sigma}D^T \\ &\quad + 2MFD\bar{\Sigma}D + 2MQC^T. \end{aligned} \quad (25)$$

Setting $(\partial J/\partial F) = 0$ implies that

$$F = -QC^T V_2^{-1} - \Gamma\bar{\Sigma}D^T V_2^{-1} \quad (26)$$

where $V_2 = D_2\sigma_\xi\sigma_\xi^T D_2^T + D\bar{\Sigma}D^T$.

Also

$$\begin{aligned}\frac{\partial J}{\partial M} &= FD_2\sigma_\xi\sigma_\xi^T D_2^T F^T + \Gamma\bar{\Sigma}\Gamma^T + 2FD\bar{\Sigma}\Gamma^T \\ &\quad + FD\bar{\Sigma}D^T F^T + QA^T + QC^T F^T + AQ + FCQ \\ &= FV_2F^T + \Gamma\bar{\Sigma}\Gamma^T + 2FD\bar{\Sigma}\Gamma^T \\ &\quad + 2QC^T F^T + QA^T + AQ. \end{aligned} \quad (27)$$

Setting $(\partial J/\partial M) = 0$ and from (27), it follows that:

$$AQ + QA^T + \Gamma\bar{\Sigma}\Gamma^T - FV_2^{-1}F^T = 0. \quad (28)$$

Equation (28) along with (26) implies (19). □

Remark 1: The JDP estimator (14), (18), and (19) is similar to the steady-state Kalman filter, but an additional term $(\Gamma + FD)\lambda\mu_\eta$ is added. The additional term can potentially improve the dynamic response of the filter, and thus is able to capture abrupt changes such as road anomalies. In addition, the algebraic Riccati equation in (19) has more terms which encode more disturbance information.

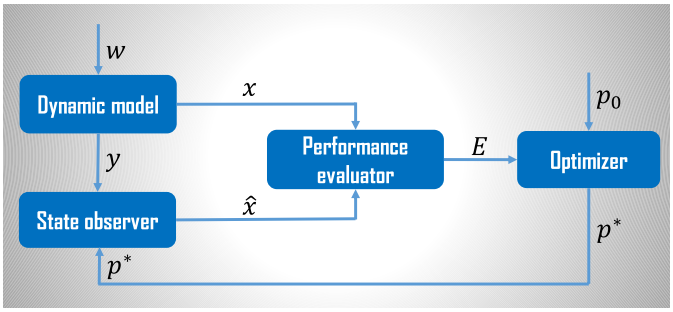

Fig. 5. Schematic framework of filter autotuning.

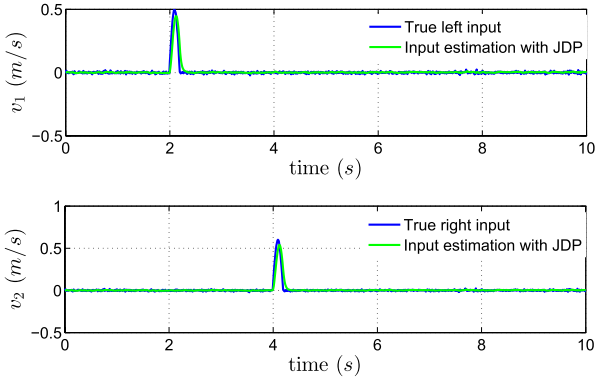

Fig. 6. Input estimation with the JDP estimator.

2) Comparison With Kalman Filter: In this section, we simulate and compare state estimation and resulting input estimation performance of a Kalman filter and the JDP-based estimator. To better compare these two state observers, an autotuning framework, as shown in Fig. 5, is applied to tune parameters for the two filters. The parameter optimization is based on simulations with the disturbance w specified as the blue line in Fig. 6 and we let $u = 0$. The disturbance w is then fed into the dynamic system (7) to obtain "true" state x and system output y. With output y and assumed observer parameters, the observer will generate a state estimate $\hat{x}$. A performance evaluator then compares true state x and state estimate $\hat{x}$, and generates an estimation performance metric E. An optimizer is exploited to iteratively optimize the parameters based on the performance metrics.

In this paper, we use the root-mean-square of $x - \hat{x}$ as the performance metric and we exploit MATLAB *fmincon* function as the optimizer. To increase the likelihood that a global minimizer is found, we run the optimizer with 20 random initial conditions p_0.

The Kalman filter parameters to be optimized are the process noise covariance matrix $W \in \mathbb{R}^{4\times4}$ and the measurement noise covariance $V \in \mathbb{R}^{3\times3}$. To reduce the number of parameters to be optimized, we optimize diagonal matrices for W and V. The optimized Kalman filter parameters are $W = \text{diag}\{7.3, 4.2, 1.5, 9\}$ and $V = 10^{-3} \cdot \text{diag}\{0.11, 1.21, 0.81, 0.34\}$.

TABLE I
JDP-BASED ESTIMATOR PARAMETERS

μ_η	Σ_η	σ_ζ	σ_ξ	λ
$[3.1, 1.5]$	$3.3 \cdot \mathbf{I}_2$	$7.8 \cdot \mathbf{I}_2$	$0.011 \cdot \mathbf{I}_2$	0.01

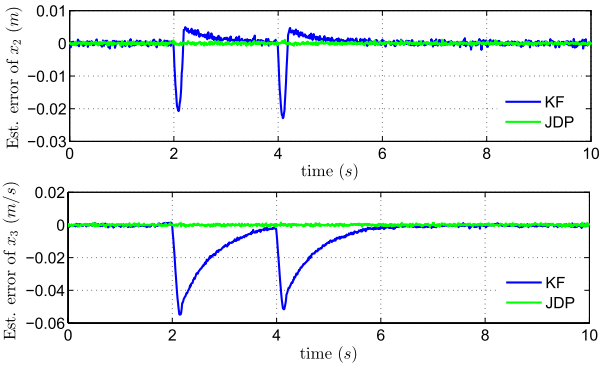

Fig. 7. State estimation error with KF and JDP estimator.

The parameters of the JDP estimator to be tuned include the mean jump size $\mu_\eta \in \mathbb{R}^{2\times 1}$, covariance matrix of the jump $\Sigma_\eta \in \mathbb{R}^{2\times 2}$, covariance matrix of the Wiener processes $\sigma_\zeta \mathbb{R}^{2\times 2}$ and $\sigma_\eta \in \mathbb{R}^{2\times 2}$, and the jump rate $\lambda \in \mathbb{R}$. Similar to simplify the autotuning, we assume that the matrices Σ_η, σ_ζ, and σ_η are scalars times an identity matrix. The optimized parameters are listed in Table I.

Note that we autotune the parameters for the two filters with the same system perturbation, i.e., $u = 0$, and w from Fig. 6. The reason is that this JDP-like perturbation w is what we expect to encounter for the road anomaly detector and it is what we would like to optimize on. The subsequential performance comparisons are also based on JDP-like perturbations.

With the optimized parameters for both Kalman filter and the JDP-based state observer, we first present a performance comparison by simulating the response of hitting a pothole. A pothole can be modeled as an input for which a jump occurs at one wheel while the other one is flat. Fig. 6 shows an example, where a left pothole at 2 s and a right pothole at 4 s are encountered. Note that this disturbance profile is actually rapidly changing over time. It looks flat except for the jumps because of the relatively small magnitude compared with the jumps. With the specified inputs in Fig. 6, the state estimation errors for x_2 and x_3 are shown in Fig. 7. Note that x_1 and x_4 are included in the measurement output in the simulations.

Fig. 7 suggests that the JDP-based estimator provides an improved performance compared with Kalman filter, while Figs. 6 and 8 indicate that the combined scheme with the input observer performs better when potholes occur, i.e., at around 2 and 4 s.

We next present a performance comparison in the case where the vehicle hits a speed bump. A speed bump can be modeled as an input, where both wheels have jumps with similar magnitudes. See Fig. 9 as an example where a speed bump is encountered at 2 s. State estimation errors are shown in Fig. 10. The JDP-based estimator tracks the true states well, while the Kalman filter does not work well during and immediately following the jumps.

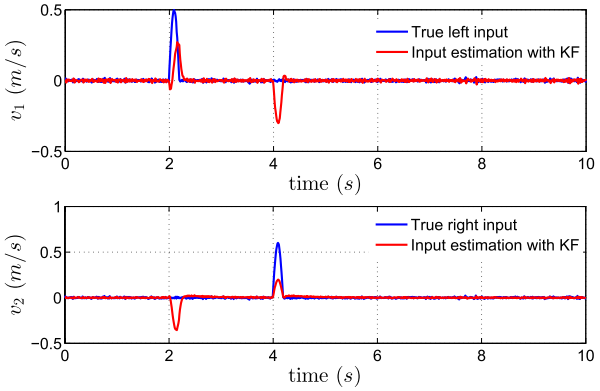

Fig. 8. Input estimation with the KF.

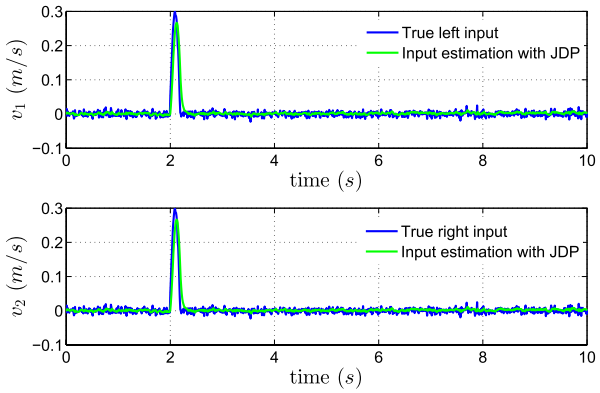

Fig. 9. Input estimation with the JDP estimator.

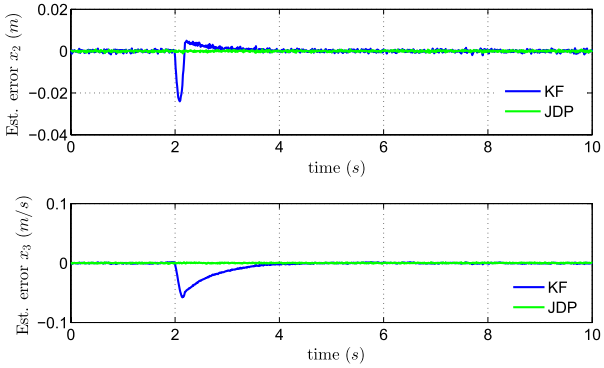

Fig. 10. State estimation error with KF and JDP estimator.

Consequently, as shown in Fig. 9, the inputs with a JDP-based state estimator are tracked well, while the jumps are tracked poorly with the Kalman filter, as shown in Fig. 11.

D. Detection Logic

In this section, we apply the JDP-based estimator developed in Section III-C to road anomaly detection. The algorithm can also label the anomaly types, such as potholes, speed bumps, and road joints.

We showed that the JDP-based state estimator (14) coupled with the input observer (9) can be exploited to estimate road

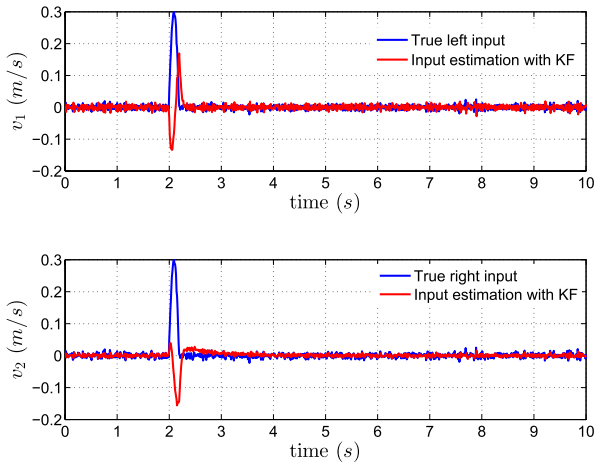

Fig. 11. Input estimation with the KF.

Algorithm 1 Road Anomaly Detection Algorithm

Inputs: $\hat{v}_1$, $\hat{v}_2$, $\bar{v}$, t_{p2p}, $\mathcal{L}^-$

Outputs: Anomaly indication and anomaly label (left/right/large/small pothole, speed bump)

if $\mathcal{L}^- = 1$ and $t_{p2p} < L/\bar{v}$ **then**
  Report *no* anomaly.
else
  if $\hat{v}_1 > th_1(\bar{v})$ or $\hat{v}_2 > th_1(\bar{v})$ **then**
    if $\frac{|\hat{v}_1 - \hat{v}_2|}{\min(\hat{v}_1, \hat{v}_2)} < th_{perc}$ **then**
      speed bump detected.
    else if $\hat{v}_1 > \hat{v}_2$ **then**
      left large pothole detected.
    else
      right large pothole detected.
  else if $\hat{v}_1 > th_2(\bar{v})$ or $\hat{v}_2 > th_2(\bar{v})$ **then**
    if $\frac{|\hat{v}_1 - \hat{v}_2|}{\min(\hat{v}_1, \hat{v}_2)} < th_{perc}$ **then**
      road joints detected.
    else if $\hat{v}_1 > \hat{v}_2$ **then**
      left small pothole detected.
    else
      right small pothole detected.
  else
    report *no* anomaly.

velocity inputs in Section III-C. With road velocity input estimation, Algorithm 1 is developed to detect and label road anomalies.

In the algorithm, $\hat{v}_1$ and $\hat{v}_2$ are, respectively, the maximum magnitudes of the estimated left and right road velocity inputs over the past time window. $\bar{v}$ is the average car speed over the time window; t_{p2p} denotes the peak-to-peak time duration from the last time window to the previous window; L is the car length; $\mathcal{L}^-$ is the label variable to indicate whether an anomaly was reported for the last time window. The value $\mathcal{L}^- = 1$ indicates an anomaly was reported in that time window, while $\mathcal{L}^- = 0$ indicates no anomaly was reported. The parameter th_1 is a vehicle speed-dependent threshold for large anomaly response. The parameter th_2, $th_2 < th_1$, is a vehicle speed-dependent threshold for small anomalies and th_{perc} is a threshold for the left and right input differences. In a real-time implementation, lookup tables are implemented for th_1 and th_2 as a function of average speed.

(a) (b) (c)

Fig. 12. Three road surface types; roughness increases from left to right. (a) Surface 1. (b) Surface 2. (c) Surface 3.

Since we use a front half-car model, repeated patterns can be found when the rear part of the car hits the same anomaly. An experimental example is given in Fig. 15, where the repeated patterns can be found around 3 and 5.3 s. The first *if* statement is used to differentiate the repeated pattern from a new anomaly. This is because the rear half of the car also hits the anomaly causing secondary jumps. We compare the peak-to-peak time duration t_{p2p} with car length L divided by the average speed during window $\bar{v}$. If $t_{p2p} < L/\bar{v}$, then the anomaly is not classified as a new anomaly. Otherwise, the subsequent steps are executed.

The anomaly detection algorithm is based on the fact that the pothole is an event where jump occurs on only one side while speed bumps or road joints are events where both sides have jumps. The two thresholds th_1 and th_2 are magnitude thresholds used to determine whether the response is large or small.

Note that the overall computation and memory footprint for the proposed anomaly detection system are quite light. With filter parameters being tuned offline, the optimal filter gain F is computed offline using (18). The implementation of the filter (14) is the same as an infinite-horizon Kalman filter except for an additional algebraic computation $(\Gamma + FD)\lambda\mu_\eta$, which requires little computation.

Similarly, the input observer (9) also has small computational footprint. The detection logic in Algorithm 1, however, requires a buffer for the 1-s processing window, which requires a buffer size of 100. The computation requirement for the detection logic is low. In summary, the computation and memory requirements for the proposed detection algorithm are quite small and thus suitable for real-time implementation.

IV. Experimental Results

We have shown above that the road input estimator works well in simulations. We also tested the input estimator in a 2012 Lincoln MKS test vehicle, pictured in Fig. 3. However, there is no "true" road velocity for comparison. As a result, we first test road input estimation performance by running our test vehicle on road segments with different road surface types to see whether the estimator can reflect roughness levels. Three different surfaces are shown in Fig. 12, where the roughness increases from left to right. The test vehicle was driven at approximately 30 km/h on the road segments, and left input estimations $\hat{v}_1$ are shown in Fig. 13. The results demonstrate that the input estimation algorithm is clearly sensitive to the road surface type.

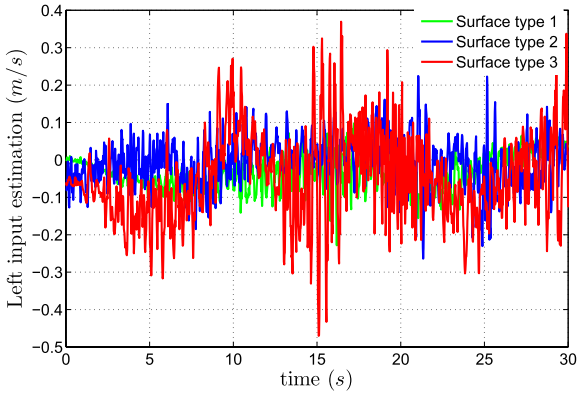

Fig. 13. Input estimation on the three road surfaces.

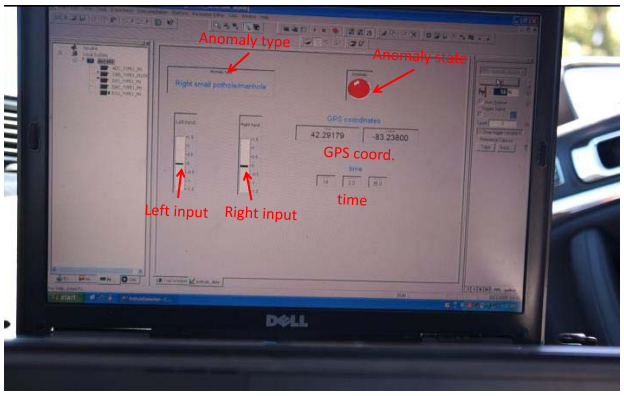

Fig. 14. Real-time dSPACE ControlDesk interface.

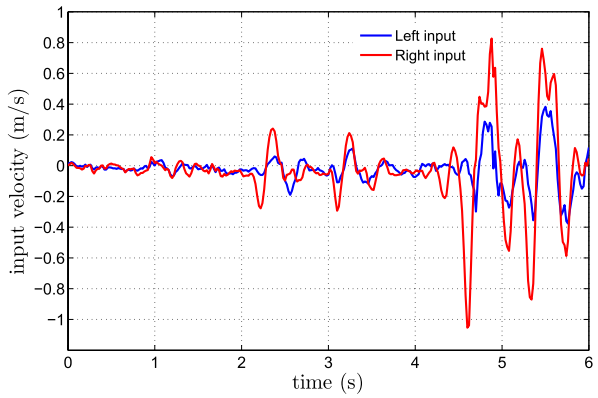

Fig. 15. Input estimation when driving over a small pothole followed by a large pothole.

Our road anomaly detection algorithm validation procedure is straightforward. We ran our detection algorithm in real time on dSPACE and an interface was used to indicate real-time detections, as shown in Fig. 14. The interface can indicate whether an anomaly has been detected (state light), the anomaly type, GPS coordinates, left and right inputs, and time. Fig. 15 shows the estimated road inputs in a vehicle test when hitting a small pothole followed by a large pothole at the right side. Jumps are detected at approximately 2 and 4.2 s. Using anomaly detection algorithm 1, a right small pothole and a right large pothole were successfully detected. Note that repeated patterns can be found at approximately 3 and 5.3 s. This is because the rear half of the car also hits the pothole

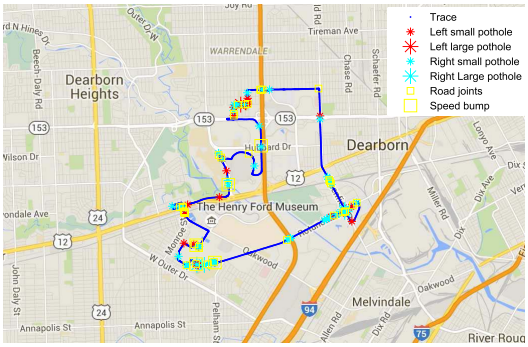

Fig. 16. Detected anomalies in Dearborn with our test vehicle.

TABLE II
SUMMARY ON ANOMALY DETECTION PERFORMANCE

False negative rate	False positive rate	Labeling accuracy
1.78%	0	86.3%

causing secondary jumps. To differentiate the repeated pattern from a new pothole, we compare the peak-to-peak time duration t_{p2p} with the car length L divided by the minimum speed during window $v_{\min}$. If $t_{p2p} < L/v_{\min}$, then it is not classified as a new anomaly. Otherwise, a new anomaly is detected.

As we drove our vehicle around Dearborn, Michigan, anomalies were detected and recorded. One of the trips is shown in Fig. 16. During our test drives, the algorithm did not reveal any false positives and there were only three missed detections. The missed detections were mainly due to smooth manholes and road joints, which are not true anomalies given our classifications. Anomaly labeling accuracy was 145 out of 168 correctly labeled reports. Note that some of the labeling errors were due to events such as uneven speed bumps. A summary of the detection performance is given in Table II.

We note that our test vehicle can be used as a probe vehicle for creating a detailed anomaly map. This map can be stored on a cloud and shared with drivers to better plan their routes. Anomaly map data are also useful for road agencies to efficiently maintain the roads.

V. CONCLUSION AND FUTURE WORK

In this paper, we developed and validated a method of road anomaly detection and classification. A multi-input observer was used to estimate road velocity inputs. The JDP-based estimator was exploited and shown to have better estimation performance than a Kalman filter when jumps are present. The derivation of the JDP-based estimator, complete with the proofs, has been presented, and the potential of it to lead to better estimation performance versus a conventional Kalman filter approach has been demonstrated in the context of our road anomaly detection application. The anomaly detector was implemented in real time on a test vehicle, and promising experimental results were obtained. The anomaly detection procedure can be applied to create a crowd-sourced anomaly map, which can assist drivers in route planning and help road agencies maintain the roads.

The thresholds in the detection algorithm were chosen based on a small set of experimental data. Machine learning techniques can be applied in the future to better characterize these thresholds based on a larger data set. The algorithm was only demonstrated in one vehicle. Implementation in multiple vehicles is another direction for future work.

REFERENCES

[1] S. Kou, "Jump-diffusion models for asset pricing in financial engineering," in *Handbooks in Operations Research and Management Science*, vol. 15. Amsterdam, NX, Netherlands: Elsevier, 2007, pp. 73–116.

[2] H. U. Gerber, E. S. W. Shiu, and H. Yang, "Valuing equity-linked death benefits in jump diffusion models," *Insurance, Math. Econ.*, vol. 53, no. 3, pp. 615–623, Nov. 2013.

[3] K. I. Amin, "Jump diffusion option valuation in discrete time," *J. Finance*, vol. 48, no. 5, pp. 1833–1863, Dec. 1993.

[4] D. Duffie, J. Pan, and K. Singleton, "Transform analysis and asset pricing for affine jump-diffusions," *Econometrica*, vol. 68, no. 6, pp. 1343–1376, 2000

[5] Z. Li, I. Kolmanovsky, E. Atkins, J. Lu, D. Filev, and J. Michelini, "Cloud aided semi-active suspension control," in *Proc. IEEE Symp. Comput. Intell. Vehicles Transp. Syst. (CIVTS)*, Dec. 2014, pp. 76–83.

[6] J. Eriksson, L. Girod, B. Hull, R. Newton, S. Madden, and H. Balakrishnan, "The pothole patrol: Using a mobile sensor network for road surface monitoring," in *Proc. 6th Int. Conf. Mobile Syst., Appl., Services*, 2008, pp. 29–39.

[7] Z. Li, I. Kolmanovsky, E. Atkins, J. Lu, and D. Filev, "Road anomaly estimation: Model based pothole detection," in *Proc. Amer. Control Conf.*, Jul. 2015, pp. 1315–1320.

[8] *Pothole Alert Research*, accessed on Nov. 15, 2015. [Online]. Available: http://www.landrover.com/experiences/news/pothole-detection.html

[9] U. Kalabić, I. Kolmanovsky, and J. Buckland, "Multi-input observer for estimation of compressor flow," in *Proc. ASME Dyn. Syst. Control Conf.*, 2013, p. V001T04A002.

[10] I. V. Kolmanovsky and T. L. Maizenberg, "Stochastic stability, estimation and control in systems driven by jump-diffusion disturbances and their automotive applications," in *Proc. 45th IEEE Conf. Decision Control*, Dec. 2006, pp. 4194–4199.

[11] A. Papoulis and S. Pillai, *Probability, Random Variables and Stochastic Processes* (Electrical and Electronic Engineering Series). New York, NY, USA: McGraw-Hill, 2002.

[12] F. Li, L. Wu, P. Shi, and C.-C. Lim, "State estimation and sliding mode control for semi-Markovian jump systems with mismatched uncertainties," *Automatica*, vol. 51, pp. 385–393, Jan. 2015.

[13] P. Shi, Y. Zhang, and R. K. Agarwal, "Stochastic finite-time state estimation for discrete time-delay neural networks with Markovian jumps," *Neurocomputing*, vol. 151, pp. 168–174, Mar. 2015.

[14] B. Øksendal and A. Sulem-Bialobroda, *Applied Stochastic Control of Jump Diffusions*. Springer, 2009.

[15] F. B. Hanson, *Applied Stochastic Processes and Control for Jump-Diffusions: Modeling, Analysis, and Computation*, vol. 13. Philadelphia, PA, USA: SIAM, 2007.

[16] D. Karnopp, "Active damping in road vehicle suspension systems," *Vehicle Syst. Dyn.*, vol. 12, no. 6, pp. 291–311, 1983.

[17] N. Giorgetti, A. Bemporad, H. E. Tseng, and D. Hrovat, "Hybrid model predictive control application towards optimal semi-active suspension," *Int. J. Control*, vol. 79, no. 5, pp. 521–533, 2006.

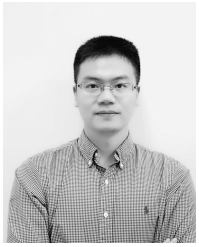

Zhaojian Li (S'15–M'16) received the B.S. degree in civil aviation from the Nanjing University of Aeronautics and Astronautics, Nanjing, China, in 2010, and the M.S. and Ph.D. degrees from the Department of Aerospace Engineering, University of Michigan, Ann Arbor, MI, USA, in 2014 and 2016, respectively.

From 2010 to 2012, he was an Air Traffic Controller with the Shanghai Area Control Center, Shanghai, China. From 2014 and 2015, he was an Intern with Ford Motor Company, Dearborn, MI, USA. Since 2013, he has been a Graduate Research Assistant with the Department of Aerospace Engineering, University of Michigan. His current research interests include optimal control, system modeling, estimation, and intelligent transportation systems.

Dr. Li was a recipient of the National Scholarship from China.

Ilya V. Kolmanovsky (F'08) received the M.S. and Ph.D. degrees in aerospace engineering and the M.A. degree in mathematics from the University of Michigan, Ann Arbor, MI, USA, in 1993, 1995, and 1995, respectively.

He was with Ford Research and Advanced Engineering, Dearborn, MI, USA. He is currently a Full Professor with the Department of Aerospace Engineering, University of Michigan. He is also an Inventor of 92 U.S. patents. His current research interests include control theory for systems with state and control constraints, and control applications to aerospace and automotive systems.

Dr. Kolmanovsky was a recipient of the Donald P. Eckman Award of American Automatic Control Council.

Uroš V. Kalabić (M'16) received the B.A.Sc. degree in engineering science from the University of Toronto, Toronto, ON, Canada, in 2010, the M.S.E. degree in aerospace engineering and the M.S. degree in mathematics from the University of Michigan, Ann Arbor, MI, USA, in 2011 and 2014, respectively, and the Ph.D. degree in aerospace engineering from the University of Michigan in 2015.

He was a Research Intern with Ford Motor Company, Dearborn, MI, USA, from 2011 to 2012, and Mitsubishi Electric Research Laboratories, Cambridge, MA, USA, in 2014. Since 2015, he has been a Research Scientist with Mitsubishi Electric Research Laboratories. His current research interests include the control of systems subject to state or output constraints and applications to aerospace and automotive systems.

Ella M. Atkins (SM'14) received the advanced Ph.D. degrees and master in aeronautics and astronautics from the Massachusetts Institute of Technology, Cambridge, MA, USA, and in computer science and engineering from the University of Michigan, Ann Arbor, MI, USA.

She is currently an Associate Professor with the Department of Aerospace Engineering, University of Michigan, where she is also the Director of the Autonomous Aerospace Systems Laboratory. She has authored over 150 refereed journal and conference publications. Her current research interests include task and motion planning, guidance, and control strategies to support increasingly autonomous cyberphysical aerospace systems.

Dr. Atkins was a member of the Institute for Defense Analyses Defense Science Studies Group from 2012 to 2013. She is the Graduate Program Chair for the new University of Michigan Robotics Program. She serves on the National Academy's Aeronautics and Space Engineering Board. She also serves as an Associate Editor of the *AIAA Journal of Aerospace Information Systems*.

Jianbo Lu (SM'09) received the Ph.D. degree in aeronautics and astronautics from Purdue University, West Lafayette, IN, USA, in 1997.

He is currently a Technical Expert in advanced vehicle controls with the Controls Research and Advanced Engineering, Research, and Innovation Center, Ford Motor Company, Dearborn, MI, USA. He has authored over 70 referred research articles. He is an Inventor or Co-Inventor of over 100 U.S. patents. His invented technologies have been widely implemented in the tens and millions of vehicles with brand names, such as Ford, Lincoln, Volvo, and Land Rover. His current research interests include automotive controls, intelligent and adaptive vehicle systems, integrated sensing systems, driving assistance and active safety systems, and future mobility.

Dr. Lu was a two-time recipient of the Henry Ford Technology Award at Ford Motor Company. He serves as the Chair of Intelligent Vehicular Systems and Control Technical Committee under the IEEE Society of Systems, Man, and Cybernetics. He also serves as an Associate Editor of the IEEE TRANSACTIONS ON CONTROL SYSTEMS TECHNOLOGY. He is on the Editorial Board of the *International Journal of Vehicle Autonomous Systems* and the *International Journal of Vehicle Performance*. From 2008 to 2014, he served as an Associate Editor of the *IFAC Journal of Control Engineering Practice*. He also served as the Vice Chair for Industry and Applications at the 2015's American Control Conference.

Dimitar P. Filev (F'08) received the Ph.D. degree in electrical engineering from Czech Technical University in Prague, Prague, Czech Republic, in 1979.

He is currently an Executive Technical Leader in intelligent controls with the Ford Motor Company, Dearborn, MI, USA, where he is involved in conducting research in modeling and control of complex systems, intelligent control, fuzzy and neural systems, and their applications to automotive engineering. He has authored four books and over 200 articles in refereed journals and conference proceedings. He holds numerous U.S. and foreign patents.

Dr. Filev was a recipient of the 2015 IEEE Computational Intelligence Society Pioneer's Award, the 2008 Norbert Wiener Award of the IEEE System, Man, and Cybernetics (SMC) Society, and the 2007 International Fuzzy Systems Association (IFSA) Outstanding Industrial Applications Award. He is the President-Elect of the IEEE SMC Society. He is a fellow of the IFSA.